Self-Assembly of Protein-Containing Lipid-Bilayer Nanodiscs from Small-Molecule Amphiphiles

Florian Mahler, Annette Meister, Carolyn Vargas, Grégory Durand, Sandro Keller

NANO · MICRO small
www.small-journal.com

Self-Assembly of Protein-Containing Lipid-Bilayer Nanodiscs from Small-Molecule Amphiphiles

Florian Mahler, Annette Meister, Carolyn Vargas, Grégory Durand, and Sandro Keller**

When membrane proteins are removed from their natural environment, the quality of the membrane-solubilizing agent used is critical for preserving their native structures and functions. Nanodiscs that retain a lipid-bilayer core around membrane proteins have attracted great attention because they offer a much more native-like environment than detergent micelles. Here, two small-molecule amphiphiles with diglucose headgroups and either a hydrocarbon or a fluorocarbon hydrophobic chain are shown to directly assemble lipids and membrane proteins to form native nanodiscs rather than mixed micelles. Self-assembly of nanodiscs of increasing complexity from both defined, artificial vesicles as well as complex, cellular membranes is demonstrated. A detailed investigation of bilayer integrity and membrane-protein activity in these nanodiscs reveals gentle effects on the encapsulated bilayer core. The fluorinated amphiphile appears particularly promising because its lipophobicity results in gentle, non-perturbing interactions with the nanoscale lipid bilayer. A sequential model of nanodisc self-assembly is proposed that proceeds through perforation of the original membrane followed by saturation and complete solubilization of the bilayer. On this basis, pseudophase diagrams are established for mixtures of lipids and nanodisc-forming diglucoside amphiphiles, and the latter are used for the extraction of a broad range of membrane proteins from cellular membranes.

1. Introduction

Integral membrane proteins are delicate targets for in vitro studies because they usually need to be extracted from their native environment while hydrophobic surfaces need to be shielded from the aqueous solution by a membrane mimic. Traditionally, detergents have been applied to extract and purify membrane proteins, although they mimic the native environment only poorly and often lead to denaturation and loss of function.[1] Lipid-bilayer nanodiscs are excellent tools for studying membrane proteins under native-like yet well-controlled in vitro conditions. Such nanodiscs encapsulate membrane proteins in a nanosized membrane patch that, in spite of its small size, provides a native-like lipid environment.[2,3] All nanodiscs have in common that their lipid-bilayer core is surrounded by a belt composed of amphiphilic molecules that serve to shield the lipid acyl chains at the rim of the patch from contact with water. Yet, different types of nanodiscs drastically differ from one another in terms of their ability to self-assemble and their dynamics once formed. On the one hand, nanodiscs encapsulated by membrane scaffold proteins (MSPs) are kinetically trapped, static structures that require solubilization by conventional detergents before the latter are removed to drive nanodisc assembly.[4] On the other hand, both bicelles ("bilayered micelles") made from certain lipid mixtures[5] as well

F. Mahler, C. Vargas, S. Keller
Molecular Biophysics
Technische Universität Kaiserslautern (TUK)
67663 Kaiserslautern, Germany

A. Meister
HALOmem and Institute of Biochemistry
Martin-Luther-Universität Halle–Wittenberg
06108 Halle (Saale), Germany

C. Vargas, S. Keller
Biophysics, Institute of Molecular Biosciences (IMB)
NAWI Graz
University of Graz
Graz 8010, Austria
E-mail: sandro.keller@uni-graz.at

The ORCID identification number(s) for the author(s) of this article can be found under https://doi.org/10.1002/smll.202103603.

DOI: 10.1002/smll.202103603

C. Vargas, S. Keller
Field of Excellence BioHealth
University of Graz
Graz, Austria

C. Vargas, S. Keller
BioTechMed-Graz
Graz, Austria

G. Durand
Equipe Chimie Bioorganique et Systèmes Amphiphiles
Institut des Biomolécules Max Mousseron
Avignon University
Avignon 84916, France
E-mail: gregory.durand@univ-avignon.fr

G. Durand
CHEM2STAB
Avignon 84916, France

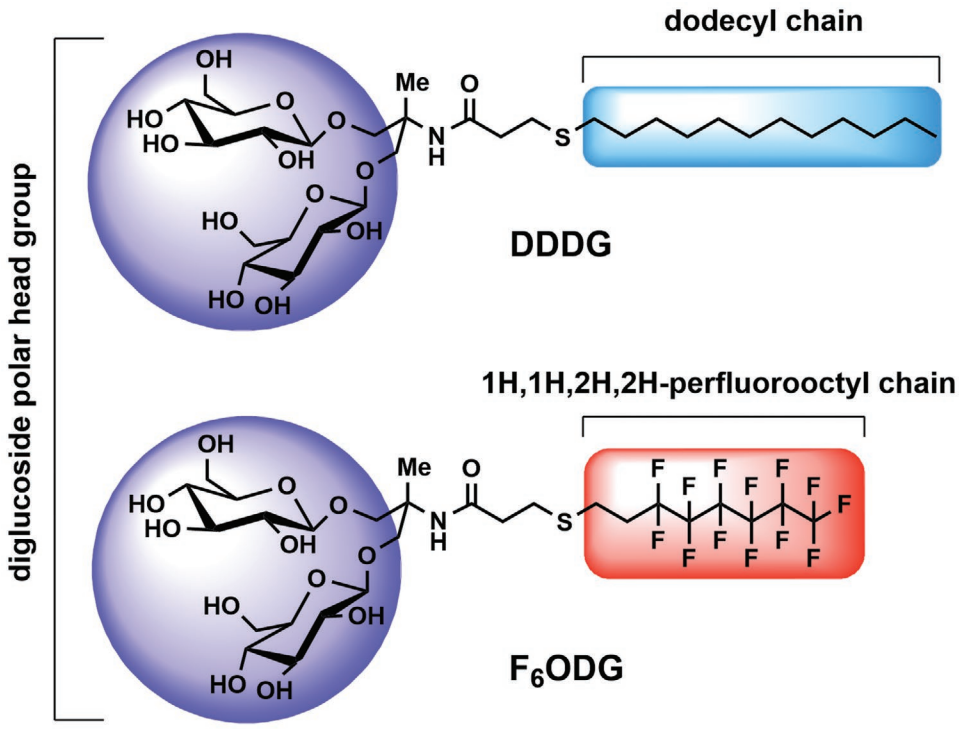

Figure 1. Chemical structures and names of nanodisc-forming diglucoside (DG) amphiphiles.

as polymer-encapsulated native nanodiscs[6] are capable of self-assembly in the absence of conventional detergents and, once formed, continue to exhibit fast dynamics of content exchange.

Here, we show that small-molecule diglucoside (DG) amphiphiles are able to recruit lipids and proteins directly into discoidal nanoparticles that retain the native-like bilayer organization of the parent membrane. Both amphiphiles possess a strongly hydrated diglucose headgroup and a hydrophobic chain and, thus, structurally resemble conventional head-and-tail detergents (**Figure 1**). While one of these amphiphiles contains a C12-hydrocarbon chain (hence, DDDG) as its hydrophobic moiety, the other carries a C8-fluorocarbon chain (hence, F_6ODG), which is expected to confer not only hydrophobicity but also lipophobicity. We have recently reported the basic physicochemical properties of two series of such detergent-like amphiphiles and their application to extract and stabilize membrane proteins in an aqueous solution.[7,8] On the one hand, a series of hydrogenated DG amphiphiles have proven superior to an established, commonly used detergent system in stabilizing essential but sensitive integral membrane proteins such as G-protein-coupled receptors (GPCRs).[8] On the other hand, a series of fluorinated DG amphiphiles have been shown to be the first fluorinated surfactants able to extract membrane proteins in amounts similar to those obtained with the aid of conventional detergents.[7]

Here, we report the unexpected finding that the solubilization of both artificial lipid vesicles and native cellular membranes by these new DG amphiphiles results in the formation of lipid-bilayer nanodiscs rather than mixed micelles. Both DG amphiphiles retain a lipid-bilayer architecture and preserve the thermotropic phase transition of saturated phospholipids yet allow rapid collisional exchange of their lipid contents. Hence, the DG amphiphiles combine the desirable features of bilayer-preserving membrane mimics with the fast dynamics typical of micelle-forming detergents. Furthermore, we demonstrate that DDDG and F_6ODG can recruit both reconstituted membrane proteins from chemically defined proteoliposomes as well as a broad range of membrane proteins directly from native cellular membranes into lipid-bilayer nanodiscs.

2. Results & Discussion

2.1. Morphology of Nanodiscs Made from Artificial Lipid Vesicles

Negative-stain transmission electron microscopy (TEM) revealed that both DG amphiphiles spontaneously formed nanodiscs when added to unilamellar lipid vesicles made from the saturated phospholipid 1,2-dimyristoyl-*sn*-glycero-3-phosphocholine (DMPC; **Figure 2**A,B). Moreover, the hydrogenated, more lipophilic DG amphiphile DDDG was also effective in accommodating the singly unsaturated phospholipid 1-palmitoyl-2-oleoyl-*sn*-glycero-3-phosphocholine (POPC) in nanodiscs (Figure 2C). Under negative-stain conditions, nanodiscs tend to form stacks—sometimes referred to as rouleaux—that are not observed in suspension. Although these stacks are staining artifacts, they allow for a straightforward analysis of some important geometrical properties of nanodiscs. Specifically, we estimated the average thickness of a nanodisc by measuring the height of a stack of nanodiscs and dividing it by the number of nanodiscs in the stack (Figure 2D). For DMPC encapsulated by F_6ODG or DDDG, we thus determined thicknesses of, respectively, (6.1 ± 0.6) nm and (5.9 ± 0.6) nm, which are typical of hydrated lipid bilayers.[9,10] For POPC encapsulated by DDDG,

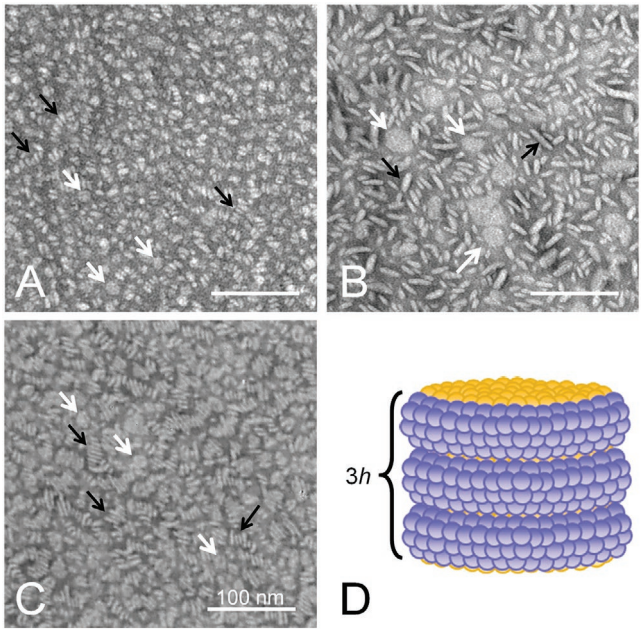

Figure 2. Formation of lipid-bilayer nanodiscs. TEM images of DG nanodiscs made from A) 0.3 mM DMPC and 1.0 mM DDDG at 30 °C, B) 0.3 mM DMPC and 0.6 mM F_6ODG at 30 °C, and C) 0.3 mM POPC and 1.0 mM DDDG at room temperature. Black arrows exemplarily indicate edge-on views of nanodiscs or nanodisc rouleaux, and white arrows point to face-on views of nanodiscs. D) Schematic measurement of bilayer thickness exploiting rouleaux formation.

we determined a thickness of (4.9 ± 0.5) nm, which is in good agreement with literature values.[9] These observations indicate that the thickness of DG nanodiscs is largely determined by the encapsulated lipids rather than the amphiphile surrounding them, which may be important for accommodating structurally and functionally diverse membrane proteins within a near-native lipid environment.

2.2. Preservation of Lipid Bilayers in Nanodiscs

2.2.1. Thermotropic Lipid Phase Transitions in Nanodiscs

Membrane proteins are embedded in a lipid bilayer; therefore, the structure and dynamics of the lipid molecules in the bilayer have a direct influence on the membrane protein. Thus, an essential criterion for gauging the usefulness of any nanodisc system is the extent to which it affects the structure and dynamics of the lipid molecules it harbors. To address this point, we exploited the main gel-to-fluid phase transition of the fully saturated phospholipid DMPC. At atmospheric pressure, this transition takes place around T_m = 24 °C and, therefore, is readily monitored by various kinds of spectroscopy and calorimetry. Here, we exploited the fluorescence properties of the membrane probe 6-dodecanoyl-2-dimethylaminonaphthalene (Laurdan), which sensitively reports on the temperature-dependent hydration state of the lipid headgroups. In particular, the influence of temperature on the hydration state of the bilayer and, consequently, the thermotropic phase transition of the membrane can be tracked by monitoring the

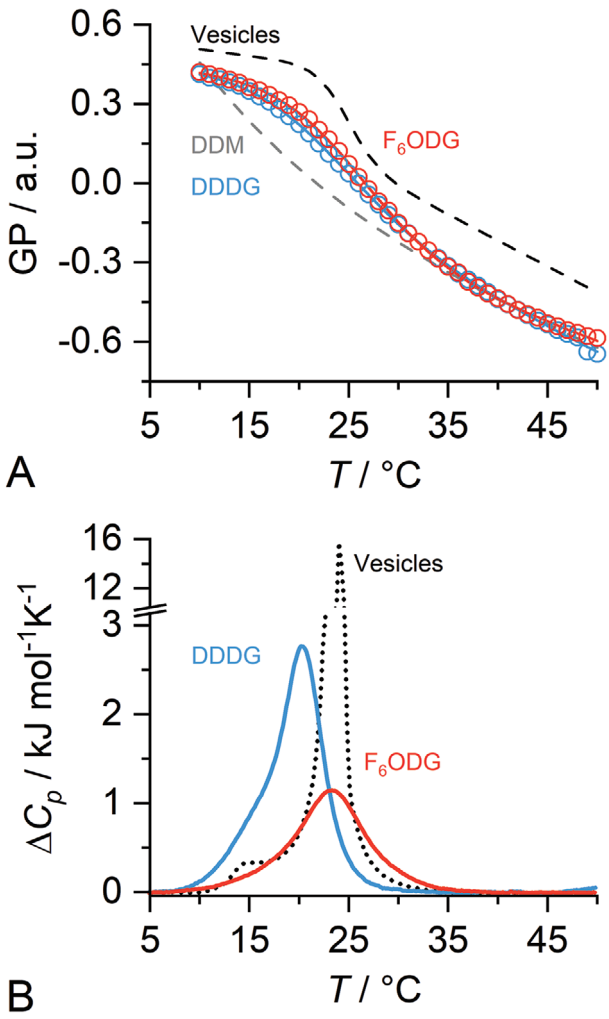

Figure 3. Gel-to-fluid phase transition of DMPC in DG nanodiscs by Laurdan fluorescence and DSC. A) Laurdan generalized polarization (GP) for hydrocarbon and fluorocarbon nanodiscs, DDM/DMPC mixed micelles, and unilamellar DMPC vesicles. DMPC (2 mM) in the form of unilamellar vesicles containing 0.5 mol% Laurdan was solubilized by addition of 5 mM DDM, 3 mM DDDG, or 3 mM F_6ODG. B) Differential isobaric heat capacity, ΔC_p, derived from DSC upscans for vesicles, hydrocarbon nanodiscs, and fluorocarbon nanodiscs. For nanodiscs, 4 mM DMPC in the form of vesicles was solubilized with 4 mM DDDG or F_6ODG.

so-called generalized polarization (GP, Equation 1, Supporting Information).[11,12] We determined T_m by fitting Equation 2 to the calculated GP values.

We thus made two major observations: First, we found only moderate changes in the inflection points of GP temperature scans, indicating minor effects of the DG amphiphiles on T_m (**Figure 3**A). In detail, T_m decreased from 24.6 °C for vesicles to 21.7 °C for DDDG and even slightly increased to 25.3 °C for F_6ODG nanodiscs. Second, the width of the transition from high GP values reflecting lower hydration in the gel phase to low GP values reflecting stronger hydration was reduced in nanodiscs as compared with vesicles, indicating a reduction in the size of the cooperative unit in the former as compared with the latter. In other words, the number of lipid molecules that undergo

the thermotropic phase transition in a cooperative manner was found to be considerably smaller in nanodiscs than in unilamellar vesicles, which is readily explained by a simple calculation: Our nanoscale lipid bilayers contain fewer than 800 lipid molecules, whereas more than 100 000 lipid molecules would be contained in a 100 nm vesicle. Further to DMPC vesicles, we used the nonionic detergent *n*-dodecyl-*β*-D-maltoside (DDM) as an additional reference that allowed us to compare DG nanodiscs with conventional detergent/lipid mixed micelles. At low temperatures, the values for both DG nanodiscs lie between those of lipid-only vesicles and mixed micelles. Above ≈30 °C, however, the hydration state of DG nanodiscs as captured by GP was found to be similar to the one of DDM/DMPC mixed micelles (Figure 3A).

We turned to differential scanning calorimetry (DSC) to study the gel-to-fluid phase transition of nanoscale phospholipid patches encapsulated by DG amphiphiles in more detail. DSC measures the difference in the isobaric heat capacity ΔC_p between the sample and a buffer reference, which results in a pronounced peak when the former undergoes a thermotropic phase transition. The dependences of T_m and the size of the cooparative unit on the DG/DMPC ratio agree well with the results from fluorescence measurements: Nanodisc formation affected T_m by only a few degrees Celsius, as reflected in a slight temperature shift of the maximum in ΔC_p (Figure 3B). Specifically, T_m decreased from 24.0 °C for vesicles to 23.4 °C and 20.2 °C for fluorocarbon and hydrocarbon nanodiscs, respectively. Again, we observed the expected decrease in the size of the cooperative unit for nanodiscs compared with vesicles, as reflected in the broadening of the transition peaks (Figure 3B). In addition, we ensured that DG nanodiscs are present below T_m, that is, when vesicular DMPC bilayers are in the gel phase. TEM of samples prepared at 10 °C (Figure S1, Supporting Information) confirmed that DG nanodiscs self-assemble at such low temperatures.

In conclusion, fluorescence and DSC experiments demonstrated that DMPC molecules in DG nanodiscs retain their characteristic main phase transition, experience rather low perturbation in their acyl chain region, and have well-hydrated headgroups above T_m. Comparing DDDG and F_6ODG, the latter turns out to be the gentler amphiphile, as one might expect from the general properties of fluorinated surfactants.[7,13] T_m is even better preserved than is the case for DMPC nanodiscs encapsulated by the amphiphilic styrene maleic acid copolymer SMA(2:1), addition of which leads to a decrease in T_m well below 20 °C.[3] Overall, these are promising properties for a nanodisc system, as membrane proteins are likely to benefit from such a near-native lipid-bilayer environment.

2.2.2. Kinetics and Mechanisms of Lipid Exchange

The kinetics and the mechanisms of lipid exchange belong to the key distinguishing properties of membrane–mimetic systems. While MSP nanodiscs exchange lipids with one another only slowly by diffusional transfer of individual lipid monomers,[14] polymer-encapsulated nanodiscs exchange lipids with each other as well as with other membrane systems much faster by collisional transfer.[15–18] Quantifying the kinetics of lipid exchange is important because it determines whether a lipid-bilayer nanoparticle represents an equilibrium or rather a kinetically trapped structure. This, in turn, has far-reaching implications for the interpretation of experiments aiming at extracting membrane proteins and lipids.

In order to monitor lipid exchange, we used two fluorescently labeled lipids, namely, *N*-(7-nitrobenz-2-oxa-1,3-diazol-4-yl)-1,2-dihexadecanoyl-*sn*-glycero-3-phosphoethanolamine (NBD-DHPE) and rhodamine B 1,2-dihexadecanoyl-*sn*-glycero-3-phosphoethanolamine (Rh-DHPE). When these lipids are colocalized within the same nanodisc, they give rise to efficient Förster resonance energy transfer (FRET). This is, the excited NBD label transfers its energy without radiation to the Rh label, which, in turn, emits light at its own characteristic emission wavelength. Using a stopped-flow device, we mixed a population of unlabeled nanodiscs containing DMPC only with a population of doubly labeled nanodiscs containing NBD-DHPE and Rh-DHPE, each at 1 mol%, and monitored time-resolved FRET (**Figure 4**A).[17] We thus found that the kinetics of donor dequenching steeply depended on the concentration of unlabeled lipid, suggesting a dominant role of collisional over diffusional lipid exchange.

Correspondingly, a global fit (Equation 3) across all lipid concentrations yielded quantitative information on the contributions of diffusional and collisional lipid exchange. In the case of diffusional lipid exchange, the lipid is transferred from one nanodisc to another by diffusion of monomers through the aqueous phase. The kinetics of this type of exchange is given by the exchange rate k_{dif}, whose value is determined by the integrity of the lipid bilayer. We found $k_{dif} = (5.35 \pm 0.02)10^{-4}$ s^{-1} for fluorocarbon nanodiscs and $k_{dif} = (93.5 \pm 0.4)10^{-4}$ s^{-1} for hydrocarbon nanodiscs. These values indicate a higher bilayer integrity in fluorocarbon nanodiscs than in hydrocarbon nanodiscs, as reflected in our observation that lipids can dissociate from the membrane more easily in the latter case. This finding fits well with the above results from fluorescence and DSC measurements that fluorocarbon nanodiscs are the milder alternative.

In addition to the exchange of individual lipid monomers, direct nanodisc/nanodisc collisions may allow for mass transfer of lipids. Here, the corresponding rate constant k_{col} reflects both the likelihood that a collisional encounter of two nanodiscs is "productive" in the sense that it allows lipid exchange and the efficiency of this kind of exchange. For fluorocarbon nanodiscs, this lipid exchange was found to be characterized by $k_{col} = (0.301 \pm 0.001)$ s^{-1} M^{-1} and for hydrocarbon nanodiscs by $k_{col} = (3.65 \pm 0.02)$ s^{-1} M^{-1}. This considerably slower collisional lipid exchange between fluorocarbon nanodiscs indicates a much stronger separation of individual bilayer patches compared with hydrocarbon nanodiscs. In the case of DMPC vesicles, this type of lipid exchange was not observed at all.

Through a comparison with other membrane mimics, it is seen that nanodiscs formed by the hydrocarbon DG amphiphile exhibited exchange rates similar to those previously observed for lipid-bilayer nanodiscs encapsulated by SMA(2:1) (Figure 4B). By contrast, fluorocarbon nanodiscs exhibited considerably slower exchange, which, however, was still more than one or two orders of magnitude faster than for MSP nanodiscs and unilamellar vesicles, respectively. The slower lipid exchange

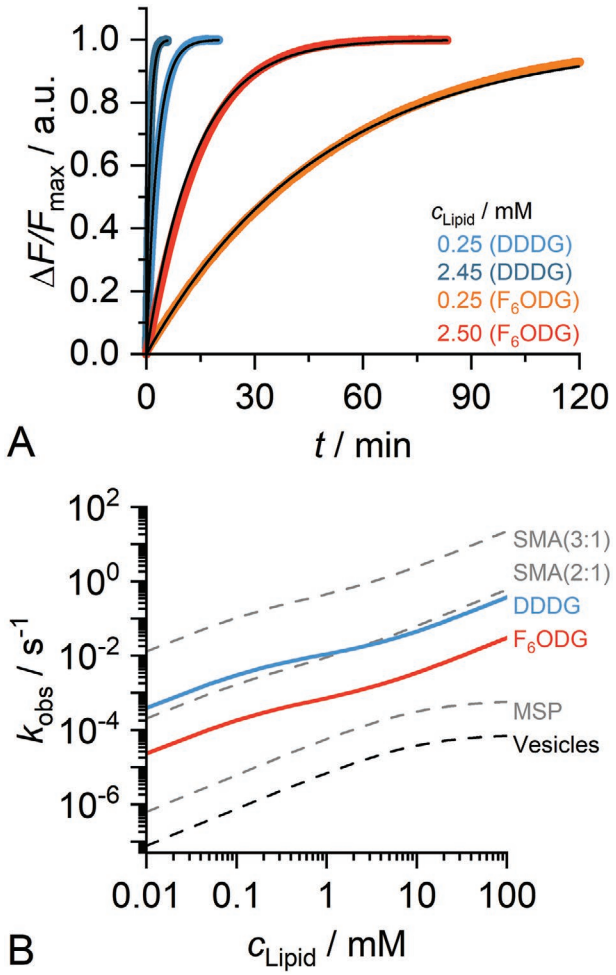

Figure 4. Investigation and comparison of lipid exchange kinetics at 35 °C. A) DMPC vesicles with and without NBD- and Rh-labeled lipids were solubilized into 25 nm-sized nanodiscs by DDDG and F_6ODG. Shown are four examples of normalized fluorescence dequenching curves. B) Resulting exchange rates of various membrane mimics across a broad range of lipid concentrations. Values for DDDG and F_6ODG were derived from the results shown in panel A. Values for SMA(3:1),[15] SMA(2:1),[18] MSP,[19] and vesicles[14] were obtained from the literature.

among MSP nanodiscs is due to the fact that they exchange lipids almost exclusively by diffusion, with negligible contributions coming from collisional exchange. The similar k_{dif} values found here for fluorocarbon nanodiscs (5.35×10^{-4} s^{-1}) and previously[19] for MSP nanodiscs (6.3×10^{-4} s^{-1}) hint at a similar degree of bilayer integrity in both nanoscale membranes. Together with their fast collisional exchange of lipid molecules, this renders fluorocarbon nanodiscs a highly promising membrane mimic that combines a near-native lipid-bilayer patch with a flexible, dynamic amphiphile belt into an equilibrium nanoparticle.

2.2.3. Mild Effects of Fluorocarbon Chains on DG Nanodiscs

Taken together, it is obvious that the fluorocarbon chains in fluorocarbon nanodiscs have a gentler effect on the bilayer properties of the core compared with the hydrocarbon chains in hydrocarbon nanodiscs. We reason that the higher T_m values (Figure 3) as compared with hydrocarbon nanodiscs are caused by (i) lower perturbation of the bilayer patch owing to a lower number of defects in lipid-bilayer packing and (ii) dehydration of the phospholipid headgroups due to slightly increased lateral pressure caused by the F_6ODG belt. Both points can be explained by a high degree of segregation between hydrocarbon lipids and fluorocarbon amphiphiles. Because lipids and lipophobic fluorocarbon compounds mix rather poorly, F_6ODG molecules are excluded from the bilayer patch and are largely restricted to the belt surrounding the nanodisc. First, this is expected to reduce the number of defects in lipid packing that otherwise would be introduced by conventional detergents. Second, this leads to a higher lateral pressure because unfavorable lipid/fluorocarbon interactions are minimized at the core/belt interface. Similar effects could also be observed by reconstitution of membrane proteins into fluorocarbon lipid bilayers, leading to higher stability of oligomers.[20,21] Furthermore, segregation explains the slower collisional lipid transfer found for fluorocarbon nanodiscs as compared with hydrocarbon nanodiscs, as the lipids have to cross the fluorocarbon belt and, thereby, would give rise to unfavorable hydrocarbon/fluorocarbon interactions. These unfavorable interactions render nanodisc/nanodisc collisions less efficient for fluorocarbon nanodiscs compared with hydrocarbon nanodiscs.

2.3. Detailed Investigation of The Solubilization Process

2.3.1. Nanodisc Self-Assembly

In order to gain a deeper understanding of the self-assembly process, we combined dynamic light scattering (DLS), NMR spectroscopy, fluorescence spectroscopy, and calorimetry to dissect the different stages leading to the formation of nanodiscs from fluid-phase DMPC at 35 °C. Considering a transition from large particles (vesicles) to small ones (nanodiscs), two straightforward parameters that can be extracted from DLS experiments are the size distribution and the average hydrodynamic diameter d_H. For vesicles in the absence of F_6ODG, we found a unimodal distribution peaking at about 100 nm as expected (**Figure 5**A). While the particle size distribution remained unimodal for all F_6ODG concentrations, we observed drastic changes in d_H. An initial increase in d_H from 100 nm to ≈2500 nm indicated vesicle aggregation upon incorporation of DG amphiphiles into the vesicular bilayer. This was followed by a drastic drop to ≈40 nm, which marked the onset of vesicle solubilization and, concomitantly, of nanodisc formation. Finally, a smooth decrease in d_H to 16 nm reflected the completion of the solubilization process (Figure 5B). Such a dependence of particle size on amphiphile concentration is well known for vesicle solubilization[22] and allows one to determine two threshold concentrations: At the saturating concentration, lipid vesicles start to disintegrate into nanodiscs because the stress induced by DG amphiphiles can no longer be accommodated in the vesicular lipid bilayer. At the solubilizing concentration, solubilization is completed, and all lipid molecules are present in the form of nanodiscs. In between these concentrations, DG

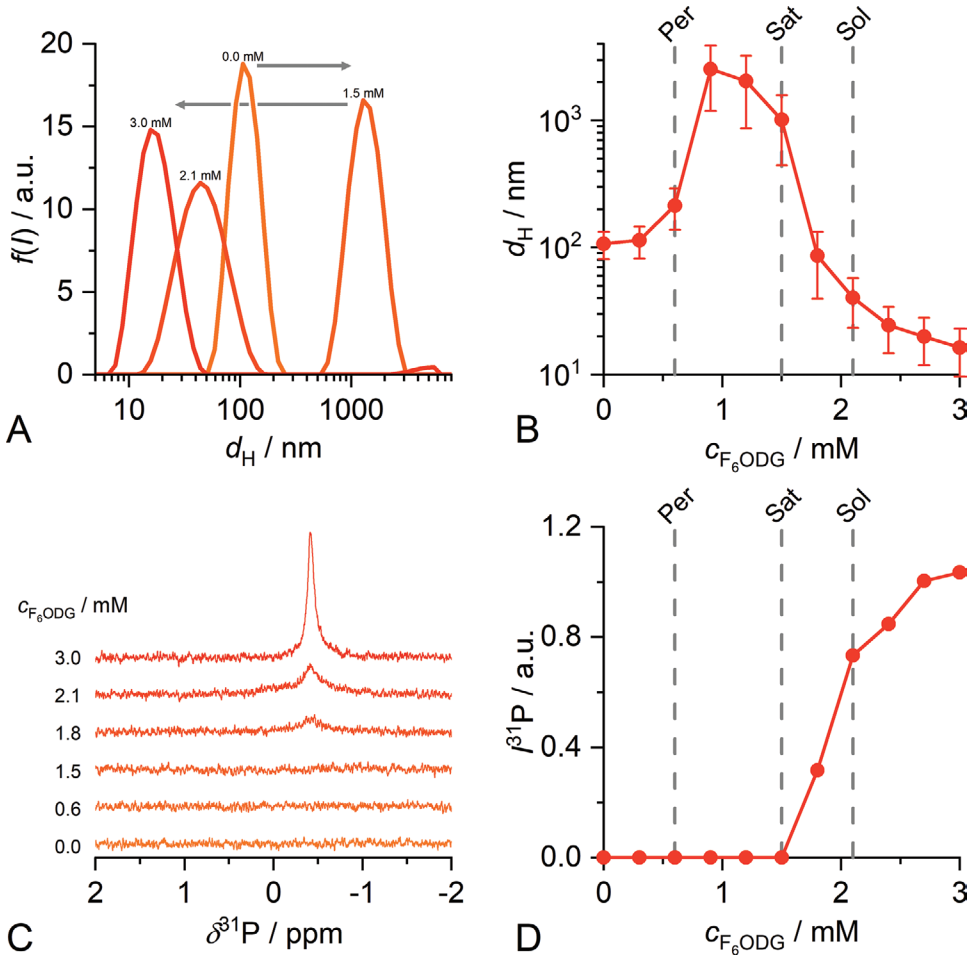

Figure 5. Solubilization of 2.8 mM DMPC vesicles with increasing F_6ODG concentrations at 35 °C. A) Intensity-weighted size distributions determined by DLS. B) Hydrodynamic diameters, d_H, derived from DLS size distributions. "Error bars" are derived from the polydispersity index. C) ^{31}P-NMR spectra of the same samples as in panel A. D) Peak intensities of ^{31}P-NMR spectra. Dashed lines indicate threshold concentrations for bilayer perforation (Per), saturation (Sat), and complete solubilization (Sol).

amphiphile-saturated vesicles and large nanodiscs coexist. In the case at hand, we thus found a saturating concentration of 1.5 mM and a solubilizing concentration of 2.1 mM F_6ODG for 2.8 mM DMPC at 35 °C.

To corroborate these values, we exploited ^{31}P-NMR, another technique that is highly sensitive to changes in the size of lipid aggregates. Lipid molecules within vesicles yield an NMR signal that is broadened beyond detection because of the slow rotational diffusion of such large structures.[23] By contrast, nanodiscs tumble much faster and, thus, give rise to a sharp ^{31}P-NMR signal. Accordingly, no peak could be detected for F_6ODG concentrations up to 1.5 mM (Figure 5C). Above this concentration, further addition of F_6ODG gave rise to an isotropic peak with increasing intensity. The break points of the resulting concentration/intensity plot agreed well with the saturation and solubilization concentrations obtained by DLS (Figure 5D). The moderate increase in the ^{31}P-NMR signal observed even beyond the solubilization was most likely due to the fact that, although solubilization was complete at this point of the titration, the nanodiscs were still relatively large (about 40 nm) and further decreased in size as more F_6ODG was added.

2.3.2. F_6ODG-Induced Lipid Vesicle Perforation

^{19}F-NMR has been applied to fluorinated surfactants in order to monitor micellization[13,7] or mixing with conventional hydrocarbon surfactants[24–26] and lipids.[13] Similarly, we used ^{19}F-NMR to monitor the change in the environment of the terminal CF_3 group of F_6ODG throughout the solubilization process. We observed a continuous change in the chemical shift to lower values with increasing F_6ODG concentrations (**Figure 6**A). The change in the chemical shift was more pronounced between 0.6 mM and 1.2 mM OF F_6ODG (Figure 6B). This shift reflected a change in the group's environment from polar to nonpolar, that is, from monomers in the aqueous solution to the bilayer-bound state. Interestingly, this pronounced change did not coincide with the saturation concentration (Figure 6B). Rather, it hints at a significant change going on in the lipid bilayer even before the latter becomes saturated with F_6ODG. This process must enable fast tumbling or flip-flopping of the incorporated F_6ODG molecules because, as mentioned above, solution NMR is insensitive to slow-tumbling nuclei. The most obvious

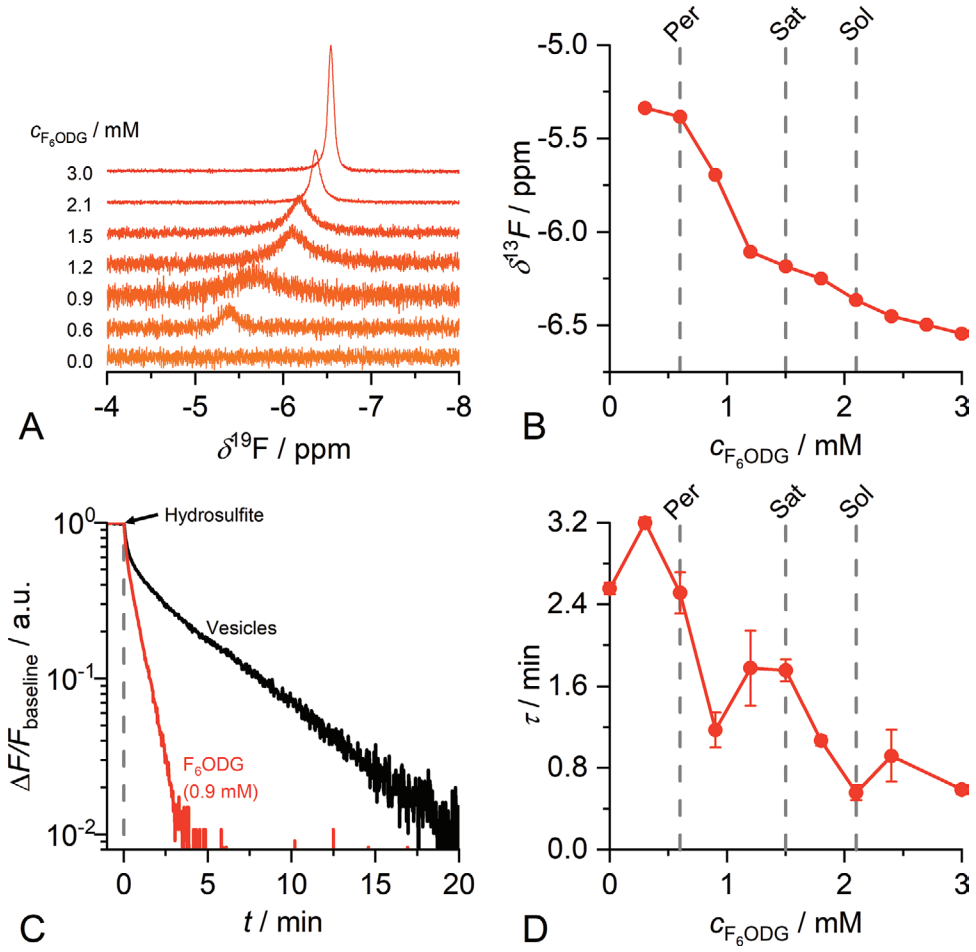

Figure 6. Detailed investigation of the solubilization process. Solubilization of 2.8 mM DMPC vesicles by increasing F_6ODG concentrations at 35 °C. A) ^{19}F-NMR spectra focusing on the peak corresponding to the CF_3 group of F_6ODG. Vertical scaling is not uniform to emphasize the shift of the maximum of the peak. B) ^{19}F-NMR chemical shifts, $\delta^{19}F$, of the CF_3 group in dependence on the F_6ODG concentration. C) Normalized NBD fluorescence as a function of the time after the addition of the bleaching agent hydrosulfite. NBD-labeled DMPC vesicles and nanodiscs were treated with hydrosulfite at timepoint zero (arrow). D) Characteristic NBD bleaching times, τ, in dependence on the F_6ODG concentration as derived from the area under the $\Delta F/F_{bl}$ curve such as those shown in panel C. Error bars are standard errors derived from replicates. Dashed lines indicate threshold concentrations for bilayer perforation (Per), saturation (Sat), and complete solubilization (Sol).

explanation for this observation would be the formation of transmembrane pores by F_6ODG. It seems particularly likely that pores may form at the interface between the bulk of the vesicular bilayer consisting of DMPC and domains rich in F_6ODG.

To test this hypothesis, we quantified the permeability of vesicular lipid bilayers to a small solute. To this end, we incubated NBD-labeled DMPC vesicles with F_6ODG and treated the samples with hydrosulfite anions to monitor the time-dependent bleaching of the NBD labels (Figure 6C). Immediately after the addition of hydrosulfite, we observed a drop in the fluorescence intensity within the first few minutes. This initial bleaching is attributed to the NBD labels on the outside of the DMPC vesicles, which are immediately accessible to hydrosulfite. Subsequently, the fluorescence intensity continued to decrease exponentially at a much slower rate. This second bleaching phase was caused by the slow diffusion of hydrosulfite through the DMPC bilayer. The time dependence of this process was captured by the characteristic bleaching time, τ. With increasing F_6ODG concentration τ decreased, indicating increasing accessibility of the interior NBD labels (Figure 6D). Closer inspection shows that the most pronounced change in τ occurred at 0.6 mM F_6ODG, where τ dropped from 2.4 min to 1.2 min. This is also the F_6ODG concentration at which ^{19}F-NMR spectroscopy revealed the most pronounced change, strongly suggesting that both methods follow the perforation of vesicular DMPC membranes upon incorporation of F_6ODG. We henceforth refer to this concentration as the perforating (Per) concentration.

2.3.3. Pseudophase Diagrams of DG Amphiphile/DMPC Mixtures

For certain applications, it is of particular importance to control the amphiphile/lipid ratio necessary to reach a desired colloidal state. On the one hand, the most common requirement in membrane-protein research might be complete solubilization. On the other hand, the perforation stage might be

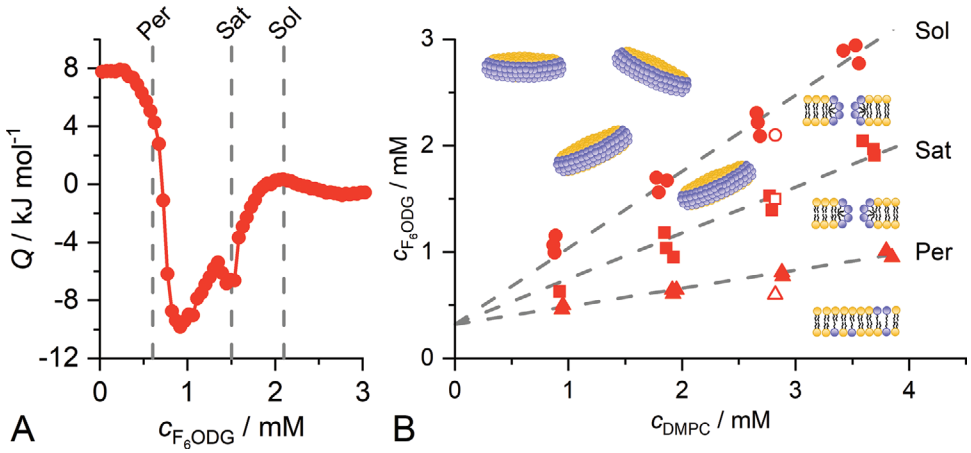

Figure 7. Pseudophase diagram of F_6ODG and DMPC. A) ITC isotherm of the solubilization of initially 3 mM DMPC by F_6ODG. Threshold concentrations obtained from other methods (i.e., DLS, NMR, and NBD bleaching) are indicated by dashed lines. B) Pseudophase diagram constructed from ITC measurements such as in panel A (solid symbols). Global fitting was performed to yield phase boundaries (dashed lines). Threshold concentrations from other methods are shown for comparison (open symbols).

interesting for other applications such as drug release. Therefore, we monitored the solubilization process for various DMPC concentrations using isothermal titration calorimetry (ITC). We titrated a concentrated DG amphiphile solution into a suspension of DMPC vesicles and measured the heat Q released upon each injection (**Figure 7**A). For all titrations, the initial injections gave rise to endothermic reactions, as often observed for membrane-partitioning processes involving nonionic small-molecule amphiphiles.[27] After a drastic drop in Q, the sign turned negative reflecting an exothermic reaction. Within this exothermic part of the self-assembly process, the thermogram followed a W shape, with the first minimum being lower than the second one. This W shape was more pronounced at higher lipid concentrations. Finally, for higher F_6ODG concentrations, a flat maximum was observed before Q declined to zero. Such complex isotherms can be explained neither in terms of a simple three-stage model nor by so-called "breaking-in"[28,29] or "staying-out"[30] mechanisms. Notwithstanding, the characteristic points observed above by DLS and ^{31}P NMR (Figure 5) as well as by ^{19}F NMR and NBD bleaching experiments (Figure 6) can be matched with the initial drop in Q (perforation), the second minimum in Q (saturation), and the flat positive maximum (solubilization). Hence, we were able to use ITC to monitor the concentration dependence of those characteristic points by performing titrations at various DMPC concentrations (Figure 7).

A systematic evaluation of all isotherms obtained at various DMPC concentrations yielded the expected linear relationships between the F_6ODG concentration resulting in a particular feature in the isotherm and the corresponding DMPC concentration (Figure 7B).[31,32,22,33] These linear relationships are described by slopes for perforation, R_{Per}, saturation, R_{Sat}, and solubilization, R_{Sol}, together with one common y-axis intercept, c_{mon} (**Table 1**). These values determine the boundaries of a pseudophase diagram that separates concentration ranges in which different colloidal states are populated. The slopes of these boundaries reflect the extreme DG/DMPC molar ratios in the various colloidal assemblies, while the y-axis intercept gives the monomer concentration, c_{mon}, of the respective DG amphiphile. c_{mon} is utterly important, as this concentration of amphiphile is always present in the aqueous phase and, therefore, needs to be considered when diluting DG nanodiscs. Potentially, these amphiphile monomers in the aqueous phase could interact directly with water-exposed parts of nanodisc-embedded membrane proteins. It is noteworthy that the pseudophase boundaries derived from different methods agree very well with one another (Figure 7B). Comparing the pseudophase boundaries obtained here (Table 1) with those previously found for SMA(2:1)/DMPC mixtures under similar conditions,[3] one can see that SMA(2:1) is the more potent solubilizing agent on a molar scale. However, comparisons of small-molecule with polymeric amphiphiles on a molar basis have to be taken with caution because of the large difference in molar mass. Comparison of the pseudophase boundaries on a mass scale (Table S1, Supporting Information) reveals that the slopes of the pseudophase boundaries are similar for the two systems, with those of the DG amphiphiles being less than twice as steep as those of SMA(2:1).

Overall, isotherms obtained by titrating DDDG into DMPC vesicles look similar (Figure S2A, Supporting Information), suggesting a similar sequence of events during the self-assembly process. In this case, however, we observed signs of large aggregates between the second minimum in Q and the flat maximum for all DMPC concentrations tested. This included reproducible shifts in the baseline heating power as well as increased noise in the raw thermogram. Thus, we were able to establish a pseudophase diagram for DDDG as well (Figure S2B, Supporting Information) by determining the same

Table 1. Parameters derived from pseudophase diagrams of DG/DMPC mixtures at 35 °C.

	F_6ODG	DDDG
R_{Per}	0.17 ± 0.06	0.11 ± 0.08
R_{Sat}	0.43 ± 0.06	0.45 ± 0.09
R_{Sol}	0.72 ± 0.06	0.82 ± 0.09
c_{mon} / mM	0.32 ± 0.14	0.12 (0.00 – 0.34)

set of parameter values detailed above. Comparison of the pseudophase boundaries (Table 1) shows that, despite its lipophobic nature, F_6ODG solubilized fluid-phase DMPC with similar efficiency as DDDG. Hence, F_6ODG not only provides a native-like lipid-bilayer environment but also turns out to be highly efficient in directly fragmenting vesicular membranes to form nanodiscs.

2.4. Model of Nanodisc Self-Assembly

On the basis of the above solubilization experiments, we propose the following sequential model of nanodisc self-assembly mediated by DG amphiphiles (Figure 7B):

In the first stage, only vesicles having an intact lipid bilayer are present. Although an increasing amount of DG amphiphile is incorporated into the bilayer upon titration with the latter, the overall structure and integrity of the lipid-bilayer membrane are not compromised. In the second stage at higher DG contents in the vesicles, the bilayer becomes perforated, that is, it loses its barrier function to polar compounds. This perforation is connected to the appearance of fast flip-flopping DG amphiphiles in the lipid bilayer (Figure 6) and is explained by the formation of transmembrane pores in or at the edge of domains rich in DG. In the third stage, the DMPC bilayers can no longer take up more DG amphiphiles, which causes solubilization and, thus, the coexistence of DG amphiphile-saturated vesicles with lipid-saturated nanodiscs (Figure 5). Finally, in the fourth stage, all DMPC is present exclusively in nanodiscs. Further addition of DG amphiphile leads to the formation of smaller nanodiscs (Figure 5B) and, ultimately, to the appearance of mixed micelles as lipids are further diluted within the colloidal assemblies.

Of course, the reason for the peculiar ability to form nanodiscs ultimately lies in the molecular structure of the DG amphiphiles. The branched arrangement of the glucose moieties leads to a large and bulky headgroup, as reflected in a high surface area per molecule observed by surface tensiometry.[34] Previous work[35] has revealed that similar amphiphiles bearing a single glucose moiety form rod-shaped micelles, whereas the DG amphiphiles studied here as well as homologous ones carrying three glucose moieties give rise to small, well-defined globular micelles in the absence of lipid. In addition, the sulfide group in the linker region of the DG amphiphiles induces a kink in the hydrophobic chain, as the C–S–C angle is known to be smaller than 100°.[36] We speculate that the decisive molecular properties that confer upon F_6ODG and DDDG the ability to form nanodiscs when combined with lipid bilayers are as follows: (i) a bulky, branched, and strongly hydrated polar headgroup, which confers high curvature, (ii) a kinked overall structure, which is expected to be poorly compatible with the relatively pronounced order within a phospholipid bilayer, and (iii) long chains that are not only hydrophobic but, in the case of F_6ODG, also lipophobic, which further enhances segregation.

2.5. Solubilization of Membrane Proteins into Nanodiscs

To explore the usefulness of hydrocarbon and fluorocarbon nanodiscs for membrane-protein research, we turned our attention to the extraction of membrane proteins from both chemically well-defined, vesicular lipid bilayers and complex, native cellular membranes. To address the first aspect, we reconstituted the bacterial membrane protein outer-membrane phospholipase A (OmpLA) into POPC vesicles and solubilized these proteoliposomes with the aid of DDDG. This treatment resulted in the formation of hydrocarbon nanodiscs having a diameter of around 25 nm, as borne out by negative-stain EM (**Figure 8**A). Moreover, we have previously found that both DG amphiphiles are able to extract membrane proteins from *Escherichia coli* membranes.[7,8] Thus, we extended our investigation of DG nanodiscs to these highly heterogeneous, native membranes. TEM images showed that F_6ODG formed native nanodiscs with a diameter of around 20 nm (Figure 8B). Moreover, it is notable that stacking, which was observed for nanodiscs formed from protein-free artificial vesicles (Figure 2), was completely suppressed by the presence of OmpLA or native *E. coli* proteins. We reason that this is chiefly due to the protrusion of soluble parts or even domains of embedded membrane proteins, which could prevent face-to-face interactions between nanodiscs encircled by DG amphiphiles (Figure 8C).

The ability to form *native nanodiscs*—that is, to recruit proteins and lipids directly from cellular membranes without abolishing the bilayer architecture of the latter—sets DG amphiphiles clearly apart from bicelle-forming amphiphiles such as DHPC or CHAPS. For this reason, we here use operational definitions of, on the one hand, *bicelles* as self-assemblies formed by small-molecule amphiphiles that are unable to extract membrane proteins directly and, on the other hand, *native nanodiscs* as self-assembled structures that do possess this highly desirable property. This is especially remarkable for F_6ODG, as fluorinated amphiphiles have long been thought to be unable to solubilize membranes. We consider the formation of bilayered nanodisc structures as opposed to mixed micelles as a possible reason for the relatively good extraction efficiency of F_6ODG as compared with other fluorinated amphiphiles, which tend to form mixed micelles.[13] Intriguingly, DDDG is even similarly efficient in extracting integral membrane proteins as the "benchmark" solubilizing agents DDM[7] and SMA(2:1)[3] (Figure S3, Supporting Information).

Further to the extraction properties, an essential aspect of using DG amphiphiles in membrane-protein research is their ability to preserve the native structures and functions of solubilized proteins once embedded into nanodiscs. We thus checked the integrity of solubilized OmpLA by SDS-PAGE and enzymatic activity measurements. Both types of DG nanodiscs were able to keep OmpLA in a folded state upon incorporation into nanodiscs, as determined by the differential migration behavior of boiled and unboiled samples in SDS-PAGE (Figure 8D). OmpLA is a phospholipase, whose enzymatic activity can be induced by the addition of divalent cations such as Ca^{2+}. The addition of $CaCl_2$ to nanodisc-embedded OmpLA resulted in an initially linear increase in absorbance reflecting a steady increase in the concentration of product (Figure 8E). While the enzymatic activity was virtually the same for OmpLA in lipid-only vesicles and fluorocarbon nanodiscs, it was slightly reduced in hydrocarbon nanodiscs. The gentler nature of F_6ODG correlates with the lower bilayer perturbation caused by its fluorocarbon chains (Figure 3 and k_{dif} values) and renders

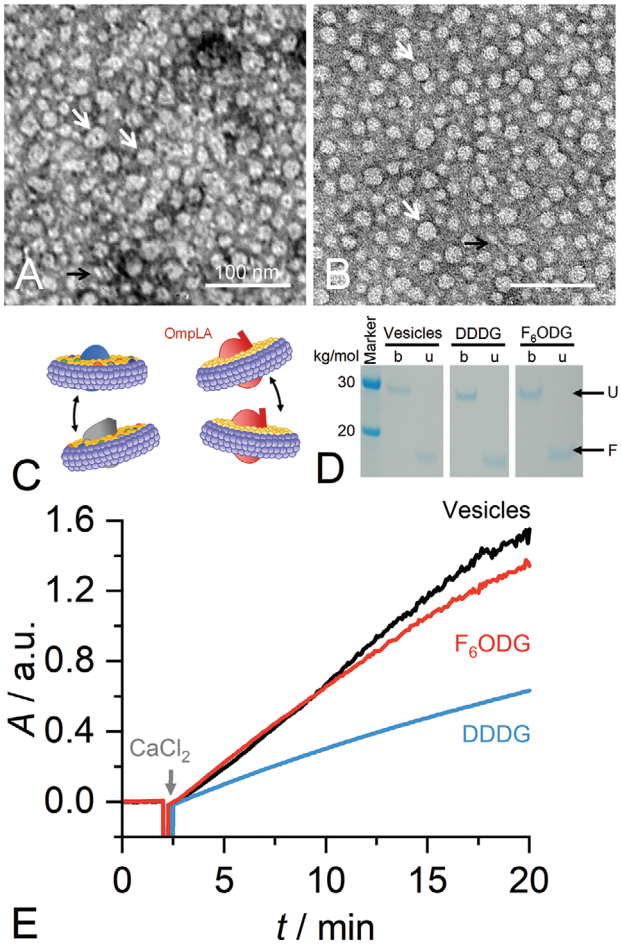

Figure 8. A,B) TEM images of DG nanodiscs made from A) 0.3 mM POPC, 1 µM OmpLA, and 1.0 mM DDDG or B) 0.25 mg ml^{-1} *E. coli* membrane and 0.2 mM F_6ODG. White arrows exemplarily indicate face-on views of nanodiscs, and black arrows indicate edge-on views of nanodiscs. C) Schematic depiction of DG nanodiscs containing the membrane protein OmpLA or complex protein/lipid mixtures. D) SDS-PAGE of OmpLA-containing samples. Boiled (b) and unboiled (u) samples were loaded to assess the folding state of OmpLA in terms of folded (F) and unfolded (U) protein. E) Ca^{2+}-induced enzyme activity measurements of OmpLA-containing vesicles, hydrocarbon nanodiscs, and fluorocarbon nanodiscs.

this compound a particularly interesting candidate for representing a new class of nanodisc-forming amphiphiles for membrane-protein research.

3. Conclusions

We have demonstrated that the diglucoside amphiphiles F_6ODG and DDDG solubilize lipids as well as protein-containing membranes to form lipid-bilayer nanodiscs rather than mixed micelles. We propose a sequential model of nanodisc self-assembly including (i) the perforation of lipid bilayers at sub-solubilizing concentrations of DG amphiphiles in the membrane, (ii) the saturation of the membrane and the onset of nanodisc formation, and (iii) the completion of the solubilization process once all lipid molecules have been transferred to nanodiscs. Contrary to bicelle-forming amphiphiles, the novel nanodisc systems presented here are capable of extracting membrane proteins directly from chemically defined, artificial proteoliposomes and, more importantly, also from highly heterogeneous, native cellular membranes. The lipophobic nature of the F_6ODG fluorocarbon chain renders the nanodiscs formed by this amphiphile remarkably gentle, as reflected by the better preservation of the bilayer architecture compared with the popular nanodisc-forming agent SMA(2:1). In summary, F_6ODG combines the advantages of (i) efficient membrane-solubilizing and protein-extracting agents, (ii) mild fluorinated surfactants having both hydrophobic and lipophobic properties, and (iii) native-like lipid-bilayer nanodiscs to provide a valuable new tool for in vitro studies of membrane proteins embedded in a nanoscale lipid bilayer (**Table 2**).

4. Experimental Section

Materials: All chemicals were obtained in the highest available purity. POPC and DMPC were kindly gifted by Lipoid (Ludwigshafen, Germany). DDDG and F_6ODG were synthesized as described elsewhere.[7,8] Tris(hydroxylmethyl)aminomethane (TRIS) and ethylenediaminetetraacetic acid (EDTA) were purchased from Carl Roth (Karlsruhe, Germany). NaCl was from VWR (Darmstadt, Germany). NBD-PE and Rhodamine-PE were purchased from Biotium

Table 2. Properties of different native nanodiscs versus other membrane mimics.

	Discoidal morphology	Lipid-bilayer core	Fast content exchange	Direct lipid solubilization	Direct protein extraction
Native nanodiscs					
F_6ODG	+	+	+	+	+
DDDG	+	+	+	+	+
SMA(2:1)	+	+	+	+	+
DIBMA	+	+	+	+	+
Other membrane mimics					
Micelle-forming detergents (e.g., DDM)	–	–	+	+	+
Bicelles	+	+	+	+/–[a)]	–
MSP nanodiscs	+	+	–	–	–

[a)]Lipid solubilization for direct formation of bicelles is limited to a narrow range of lipid compositions and experimental conditions.

(Fremont, USA). Laurdan, Na_5CO_3, H_3PO_4, $C_2F_3NaO_2$, hydrosulfite, D_2O, and 5,5'-dithiobis-(2-nitrobenzoic acid) (DTNB) were purchased from Sigma–Aldrich (Steinheim, Germany). 2-hexadecanoylthio-1-ethylphosphorylcholine (HEPC) was from Cayman Chemical (Ann Arbor, USA) and LDAO from Anatrace (Maumee, USA).

All experiments were performed in 50 mM Tris, 200 mM NaCl, and at pH 7.4, unless stated otherwise.

Vesicle Preparation: Unlabeled large unilamellar vesicles were prepared by dissolving lipid powders in buffer and shaking for several minutes. For DMPC, heating to 35 °C was required. POPC suspensions were extruded using a LiposoFast extruder (Avestin, Mannheim, Germany) at room temperature; DMPC suspensions were extruded using a Mini-Extruder (Avanti Polar Lipids, Alabaster, USA) at 35 °C. In all cases, extrusion was performed with at least 35 repeats through two stacked polycarbonate membranes with a pore diameter of 100 nm (Cytiva, Freiburg, Germany). Hydrodynamic vesicle diameters were confirmed by DLS. DMPC vesicles labeled with either 0.5 mol% Laurdan, 0.5 mol% NBD-PE, or 1 mol% NBD-PE and Rh-PE each, were prepared by dissolving the corresponding powders in chloroform, followed by mixing of DMPC and the respective dyes. Then, the chloroform was evaporated under a continuous stream of N_2 followed by drying in a vacuum desiccator overnight. Dried lipid films were resuspended in buffer and subjected to five freeze-thaw cycles with liquid N_2 to ensure homogeneous distribution. Finally, all suspensions were extruded as described above.

Transmission Electron Microscopy (TEM): Samples were prepared by mixing stock solutions to achieve the indicated concentrations and subsequent shaking overnight. Negative stained TEM samples were prepared by applying 5 µl of the sample solution to a Cu grid coated with formvar film (Plano, Wetzlar, Germany). After 1 min of incubation time, the excess sample was blotted off with filter paper. Five microliters of 1% (*w/v*) aqueous uranyl acetate solution was applied to the grid for 30 s and was blotted once more. Specimens were dried and examined on an EM 900 transmission electron microscope (Carl Zeiss Microscopy, Oberkochen, Germany), and micrographs were recorded with an SM-1k-120 slow-scan charge-coupled device (slow-scan CCD) camera (TRS, Moorenweis, Germany). The height of nanodisc stacks was measured using Fiji's (ImageJ) measure function.[37,38]

Laurdan Emission Spectroscopy: We used the fluorescence probe Laurdan in order to investigate the thermotropic phase transition of DMPC. To this end, we used a FluoTime300 spectrometer (PicoQuant, Berlin, Germany). 2 mM Laurdan-probed DMPC vesicles (cf. above) were incubated with either 3 mM DDDG, 3 mM F_6ODG, or 5 mM DDM at 35 °C overnight. All samples were excited using a 347 nm LED and perpendicular polarizer settings. Emission spectra were recorded from 380 nm to 600 nm with a detection bandwidth of 10 nm and an integration time of 1 s for temperatures of 10–50 °C with 2 min equilibration time in between. Spectra were decomposed by nonlinear least-squares fitting[39] of two Gaussian peaks corresponding to the two hydration states. Background fluorescence and scattering were negligible. Generalized polarization, GP,[11,12] was calculated as

$$\mathrm{GP} = \left(I_{440\,nm} - I_{490\,nm}\right) / \left(I_{440\,nm} + I_{490\,nm}\right) \tag{1}$$

where $I_{440\ nm}$ and $I_{490\ nm}$ are the emission intensities at 440 nm and 490 nm, respectively.

The resulting temperature dependence of GP values was then fitted by nonlinear least-square fitting according to

$$\mathrm{GP}(T) = \frac{m_1 T + b_1 - m_2 T - b_2}{1 + \exp\left(\frac{T - T_m}{\Delta T}\right)} + m_2 T + b_2 \tag{2}$$

where T denotes the experimental temperature, T_m is the phase-transition temperature, and ΔT is the width of the transition range, which was included as a fitting parameter. m_i and b_i are the slope and y-axis intercept of the pre- and post-transition baselines, respectively.

Differential Scanning Calorimetry: DSC was performed on a MicroCal VP-DSC (Malvern Instruments, Malvern, UK). DMPC (4 mM) was incubated with 4 mM DG amphiphile at 35 °C overnight. Reference and sample cells were filled with buffer and sample, respectively, before both cells were repeatedly heated and cooled. Samples containing nanodiscs were heated and cooled at a rate of 0.5 °C min^{-1}. Samples containing DMPC vesicles only were heated and cooled at a rate of 1.0 °C min^{-1}. Except for the first upscan, successive heating and cooling scans are overlaid very closely. Data were averaged, blank-subtracted, and normalized against the DMPC concentration using the MicroCal Origin 7.0 software (OriginLab, Northampton, USA). The melting temperature, T_m, was taken as the temperature at which the isobaric heat capacity difference, ΔC_p, reached its maximum.

Time-Resolved Förster Resonance Energy Transfer: Fluorescently labeled DG nanodiscs were produced by incubating 0.25 mM NBD- and rhodamine-labeled DMPC vesicles (cf. above) with DDDG and F_6ODG, respectively, in order to obtain nanodiscs with a diameter of (25 ± 5) nm, as verified by DLS (see below). Unlabeled DG nanodiscs of the same size were produced by incubating DMPC vesicles at various concentrations with corresponding DG amphiphile concentrations. Experiments were performed on an SF.3 stopped-flow apparatus (Applied Photophysics, Leatherhead, UK) equipped with a 470 nm LED and an OD 2 filter. Time-resolved donor dequenching was detected by a photomultiplier at a 90° angle at (528 ± 15) nm using an OD 6 band-pass filter (Edmund Optics, Karlsruhe, Germany). Drive syringes, tubings, and the quartz glass cell were thermostatted at 35 °C. Samples were equilibrated for at least 10 min prior to measurements. Then, 75 µl of labeled and unlabeled DG nanodiscs were mixed rapidly. Each measurement was repeated five to seven times with 1000 or 10 000 data points per repeat. The resulting traces were averaged and fitted globally as described.[17] In brief, rate constants for lipid exchange by diffusion, k_{dif}, and by collision, k_{col}, can be extracted from the equation

$$\frac{\Delta F}{F_{max}} = 1 - \exp\left(\frac{k_{dif} c_L}{c_L^0 + c_L} + k_{col} c_L\right) \tag{3}$$

Here, $\Delta F/F_{max}$ is the normalized fluorescence intensity change. k_{dif} and k_{col} are treated as global fitting parameters, while c_L and c_L^0 are the lipid concentrations of unlabeled and labeled DG nanodiscs, respectively, specific to the particular experiment. Best-fit parameter values and corresponding to 95% confidence intervals were obtained by nonlinear least-square fitting using Excel (Microsoft, Redmond, USA) as described in detail elsewhere.[39]

Dynamic Light Scattering: Measurements were performed on a Nano Zetasizer ZS90 (Malvern Instruments, Malvern, UK) equipped with a He–Ne laser and a detection angle of 90° using a 45 µl quartz glass cuvette (Hellma, Müllheim, Germany). Measurements were performed at 25 °C for POPC and at 35 °C for DMPC after both the instrument and the cuvettes had equilibrated at the respective temperature.

NMR Spectroscopy: Experiments were performed on an Avance 600 spectrometer (Bruker BioSpin, Rheinstetten, Germany) operating at a ^{31}P resonance frequency of 242.9 MHz and a ^{19}F resonance of 564.6 MHz. For all measurements, 2.8 mM DMPC vesicles (cf. above) were incubated with 0–3 mM F_6ODG at 35 °C overnight before being transferred into NMR tubes. All samples contained 10% (v/v) D_2O as a lock signal. Samples were incubated at 35 °C for 20 min inside the spectrometer prior to measurements. ^{31}P spectra were acquired with 265 scans per sample. We applied a 5 mm broadband inverse probe, an inverse-gated gated ^1H decoupling pulse sequence with an acquisition time of 1.5 s, a sweep width of 7310 Hz, and a relaxation delay of 2 s. Data were multiplied by an exponential function with a line-broadening factor of 1.0 Hz before Fourier transformation. ^{19}F spectra were acquired with 128 scans per sample. We also applied a 5-mm broadband inverse probe, an inverse gated ^1H decoupling pulse sequence with an acquisition time of 2.2 s, a sweep width of 45 045 Hz, and a relaxation delay of 1 s. Data were multiplied by an exponential function with a line-broadening factor of 0.3 Hz before Fourier transformation. ^{31}P and ^{19}F chemical shifts were referenced to H_3PO_4 and $C_2F_3NaO_2$ in D_2O, respectively, as external standards at 0 ppm. Peak areas and chemical shifts were obtained by using the TopSpin 4.0.8 software (Bruker BioSpin).

NBD Bleaching Assay: Experiments were performed on a FLUOstar Omega (BMG Labtech, Ortenberg, Germany) using its fluorescence intensity mode with λ_{ex} = 485 nm and λ_{em} = 520 nm. For all measurements, 2.8 mM NBD-labeled DMPC vesicles (cf. above) were incubated with 0–3 mM F_6ODG at 35 °C overnight. A total of 148.5 µl of each sample was transferred to a flat-bottomed 96-well microplate (Greiner Bio-One, Kremsmünster, Austria) and measured every 2 s. After 10 min, 1.5 µl of a 1 M hydrosulfite solution was added to each well, resulting in a final concentration of 10 mM hydrosulfite and ≈2.8 mM DMPC/NBD-PE, and the plate was shaken for 2 s. Measurements continued for about 20 min. Fluorescence intensity decays were normalized in order to eliminate concentration errors and scattering artifacts. To this end, the average values of the last 5 min of each measurement were subtracted and the result was divided by the average value of the initial 10 min baseline. Due to this normalization, the characteristic bleaching time τ could be directly obtained from numerical integration of the values from 10 to 30 min.

Isothermal Titration Calorimetry: All experiments were performed on an iTC200 (Malvern Instruments, Malvern, UK) in 50 mM Tris, 200 mM NaCl at pH 7.4 at 35 °C. The sample cell was loaded with 1–4 mM DMPC vesicles (cf. above) and the syringe with the respective DG amphiphile. For all experiments, a first injection of 0.4 µl was followed by 80 injections of 0.5 µl, and time spacings were chosen long enough to allow baseline re-equilibration before the next injection. Baseline subtraction and peak integration were performed using NITPIC.[40] The first injection was omitted from further analysis.

Preparation of OmpLA-Containing Vesicles: Vesicles containing outer membrane phospholipase A, OmpLA, were prepared by drop dilution of 3.22 mg ml^{-1} OmpLA in 12 mM LDAO into 1 mM POPC vesicles (cf. above) in 20 mM Tris and 2 mM EDTA at pH 8.3 to a final volume of 500 µl (20 times 0.78 µl) under permanent agitation (900 rpm) at 20 °C. After overnight incubation at 4 °C, OmpLA-containing vesicles were dialyzed for 24 h against a 500-fold excess volume of 50 mM Tris, 2 mM EDTA, and 200 mM NaCl at pH 7.4.

Escherichia coli Solubilization: *E. coli* BL21(DE3) cells were transformed with an empty pET-24 vector and selected by kanamycin resistance. After overnight incubation at 37 °C in LB medium under permanent agitation, cells were harvested and washed twice with saline by centrifugation. The resulting pellets were resuspended in ice-cold alkaline buffer (100 mM Na_5CO_3, pH 11.5) and sonicated two times for 10 min with an MS-73 SonoPlus tip sonicator (Bandelin, Berlin, Germany). Cell debris was removed by centrifugation for 30 min at 4 °C and 1000 × *g*. For separation of membrane fragments from soluble and peripheral proteins, the supernatant was ultracentrifuged for 1 h at 4 °C and 100 000 × *g*. The resulting pellets were resuspended in Tris buffer and ultracentrifuged again. Washed pellets were resuspended in Tris buffer containing complete protease inhibitor (Roche, Basel, Switzerland). Final membrane concentrations were 100 mg ml^{-1}. *E. coli* membrane suspensions were mixed with F_6ODG to final concentrations of 0.25 mg ml^{-1} membrane and 0.2 mM F_6ODG. The resulting samples were shaken at room temperature overnight.

OmpLA activity assay: The activity of OmpLA in vesicles and DG nanodiscs was monitored by a spectrophotometric assay. To this end, we solubilized OmpLA-containing vesicles with DG amphiphile stock solutions in a 1:5 ratio (proteoliposome/DG amphiphile) and incubated them for 24 h at 20 °C. In the case of F_6ODG, we heated the samples to 45 °C to ensure solubilization of the POPC vesicles. After equilibration at 20 °C for at least 1 h, samples were mixed with enzyme activity buffer containing 50 mM Tris, 150 mM NaCl, 1.3 mM HEPC, and 1.0 mM DTNB in a 3:7 ratio (buffer/sample). Samples were then incubated at 20 °C for another 2 h. Absorption measurements were performed on a Jasco V-630 UV-VIS spectrometer (Jasco Germany, Groß-Umstadt, Germany) at 412 nm using a 3 mM quartz glass cuvette (Hellma). Before inducing the color reaction via the addition of 20 mM Ca^{2+} each sample was measured for 2 min to determine the baseline absorption that was set to 0. After the addition of Ca^{2+} OmpLA could dimerize and hydrolyze HEPC, products of which, in turn, react with DTNB[41,42] and could be observed via spectroscopy.

Supporting Information

Supporting Information is available from the Wiley Online Library or from the author.

Acknowledgements

The authors are indebted to Dr. Harald Kelm and Prof. Dr. Michael Schroda (both TUK) for providing access to NMR spectroscopy and a plate reader, respectively. The authors thank Johannes Klingler (TUK) and Kevin Janson (Martin-Luther-Universität Halle–Wittenberg) for helpful comments and discussions on solubilization experiments and NBD fluorescence experiments, respectively. This work was partly funded by the Agence Nationale de la Recherche (ANR) through LabCom Chem2staB (ANR14-LAB7-0002-01) as well as by the ANR and the Deutsche Forschungsgemeinschaft (DFG) through the French–German FLUOR initiative (GD: ANR-16-CE92-0001; AM: ME 4165/2-1; SK: KE 1478/7-1).

Conflict of Interest

The authors declare no conflict of interest.

Data Availability Statement

Research data are not shared.

Keywords

fluorinated surfactants, membrane proteins, protein solubilization, self-assembly, small-molecule amphiphiles

Received: June 20, 2021
Revised: August 24, 2021
Published online: October 21, 2021

[1] R. M. Garavito, S. Ferguson-Miller, *J. Biol. Chem.* **2001**, *276*, 32403.
[2] T. H. Bayburt, Y. V. Grinkova, S. G. Sligar, *Nano Lett.* **2002**, *2*, 853.
[3] A. Grethen, A. O. Oluwole, B. Danielczak, C. Vargas, S. Keller, *Sci. Rep.* **2017**, *7*, 11517.
[4] F. Hagn, M. L. Nasr, G. Wagner, *Nat. Protoc.* **2018**, *13*, 79.
[5] A. A. de Angelis, S. J. Opella, *Nat. Protoc.* **2007**, *2*, 2332.
[6] S. Scheidelaar, M. C. Koorengevel, C. A. van Walree, J. J. Dominguez, J. M. Dörr, J. A. Killian, *Biophys. J.* **2016**, *111*, 1974.
[7] G. N. M. Boussambe, P. Guillet, F. Mahler, A. Marconnet, C. Vargas, D. Cornut, M. Soulié, C. Ebel, A. Le Roy, A. Jawhari, F. Bonneté, S. Keller, G. Durand, *Methods* **2018**, *147*, 84.
[8] P. Guillet, F. Mahler, K. Garnier, G. N. M. Boussambe, S. Igonet, C. Vargas, C. Ebel, M. Soulié, S. Keller, A. Jawhari, G. Durand, *Langmuir* **2019**, *35*, 4287.
[9] N. Kučerka, M.-P. Nieh, J. Katsaras, *Biochim. Biophys. Acta, Biomembr.* **2011**, *1808*, 2761.
[10] D. Marsh, *Handbook of Lipid Bilayers*, CRC Press, Boca Raton, FL **2013**.
[11] T. Parasassi, G. de Stasio, G. Ravagnan, R. M. Rusch, E. Gratton, *Biophys. J.* **1991**, *60*, 179.
[12] F. M. Harris, K. B. Best, J. D. Bell, *Biochim. Biophys. Acta, Biomembr.* **2002**, *1565*, 123.

[13] E. Frotscher, B. Danielczak, C. Vargas, A. Meister, G. Durand, S. Keller, *Angew. Chem., Int. Ed. Engl.* **2015**, *54*, 5069.
[14] M. Nakano, M. Fukuda, T. Kudo, H. Endo, T. Handa, *Phys. Rev. Lett.* **2007**, *98*, 238101.
[15] R. Cuevas Arenas, B. Danielczak, A. Martel, L. Porcar, C. Breyton, C. Ebel, S. Keller, *Sci. Rep.* **2017**, *7*, 45875.
[16] B. Danielczak, S. Keller, *Eur. Polym. J.* **2018**, *109*, 206.
[17] B. Danielczak, S. Keller, *Methods* **2020**, *180*, 27.
[18] A. Grethen, D. Glueck, S. Keller, *J. Membr. Biol.* **2018**, *251*, 443.
[19] M. Nakano, M. Fukuda, T. Kudo, M. Miyazaki, Y. Wada, N. Matsuzaki, H. Endo, T. Handa, *J. Am. Chem. Soc.* **2009**, *131*, 8308.
[20] H. Takahashi, M. Yoshino, K. Morita, T. Takagi, Y. Yokoyama, T. Kikukawa, H. Amii, T. Kanamori, M. Sonoyama, *Biochim. Biophys. Acta, Biomembr.* **2019**, *1861*, 631.
[21] M. Yoshino, T. Kikukawa, H. Takahashi, T. Takagi, Y. Yokoyama, H. Amii, T. Baba, T. Kanamori, M. Sonoyama, *J. Phys. Chem. B* **2013**, *117*, 5422.
[22] D. Lichtenberg, E. Opatowski, M. M. Kozlov, *Biochim. Biophys. Acta, Biomembr.* **2000**, *1508*, 1.
[23] M. Roux, P. Champeil, *FEBS Lett.* **1984**, *171*, 169.
[24] P. Barthélémy, V. Tomao, J. Selb, Y. Chaudier, B. Pucci, *Langmuir* **2002**, *18*, 2557.
[25] E. Frotscher, J. Höring, G. Durand, C. Vargas, S. Keller, *Anal. Chem.* **2017**, *89*, 3245.
[26] L. Nordstierna, I. Furó, P. Stilbs, *J. Am. Chem. Soc.* **2006**, *128*, 6704.
[27] H. Heerklotz, J. Seelig, *Biophys. J.* **2000**, *78*, 2435.
[28] A. Hildebrand, R. Neubert, P. Garidel, A. Blume, *Langmuir* **2002**, *18*, 2836.
[29] H. Heerklotz, *Biophys. J.* **2001**, *81*, 184.
[30] H. Y. Fan, D. Das, H. Heerklotz, *Langmuir* **2016**, *32*, 11655.
[31] D. Lichtenberg, H. Ahyayauch, A. Alonso, F. M. Goñi, *Trends Biochem. Sci.* **2013**, *38*, 85.
[32] D. Lichtenberg, H. Ahyayauch, F. M. Goñi, *Biophys. J.* **2013**, *105*, 289.
[33] H. Heerklotz, *Q. Rev. Biophys.* **2008**, *41*, 205.
[34] M. Abla, G. Durand, B. Pucci, *J. Org. Chem.* **2008**, *73*, 8142.
[35] C. Breyton, F. Gabel, M. Abla, Y. Pierre, F. Lebaupain, G. Durand, J.-L. Popot, C. Ebel, B. Pucci, *Biophys. J.* **2009**, *97*, 1077.
[36] T. Iijima, S. Tsuchiya, M. Kimura, *Bull. Chem. Soc. Jpn.* **1977**, *50*, 2564.
[37] J. Schindelin, I. Arganda-Carreras, E. Frise, V. Kaynig, M. Longair, T. Pietzsch, S. Preibisch, C. Rueden, S. Saalfeld, B. Schmid, J.-Y. Tinevez, D. J. White, V. Hartenstein, K. Eliceiri, P. Tomancak, A. Cardona, *Nat. Methods* **2012**, *9*, 676.
[38] C. A. Schneider, W. S. Rasband, K. W. Eliceiri, *Nat. Methods* **2012**, *9*, 671.
[39] G. Kemmer, S. Keller, *Nat. Protoc.* **2010**, *5*, 267.
[40] S. Keller, C. Vargas, H. Zhao, G. Piszczek, C. A. Brautigam, P. Schuck, *Anal. Chem.* **2012**, *84*, 5066.
[41] N. Dekker, K. Merck, J. Tommassen, H. M. Verheij, *Eur. J. Biochem.* **1995**, *232*, 214.
[42] G. L. Ellman, *Arch. Biochem. Biophys.* **1959**, *82*, 70.